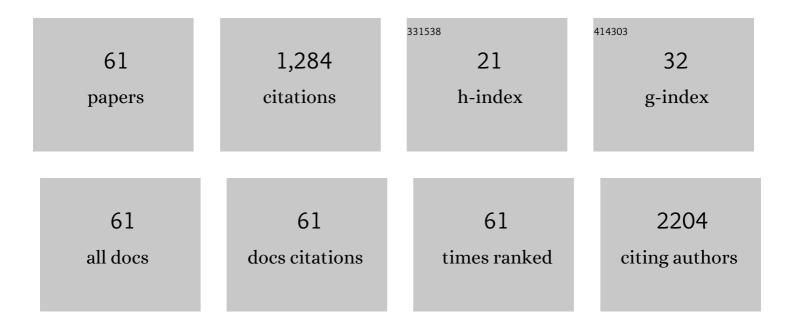
Bram Coolen

List of Publications by Year in descending order

Source: https://exaly.com/author-pdf/9070572/publications.pdf Version: 2024-02-01



#	Article	IF	CITATIONS
1	<scp>Wholeâ€Heart 4D</scp> Flow <scp>MRI</scp> for Evaluation of Normal and Regurgitant Valvular Flow: A Quantitative Comparison Between <scp>Pseudo‧piral</scp> Sampling and <scp>EPI</scp> Readout. Journal of Magnetic Resonance Imaging, 2022, 55, 1120-1130.	1.9	4
2	Higher spatial resolution improves the interpretation of the extent of ventricular trabeculation. Journal of Anatomy, 2022, 240, 357-375.	0.9	15
3	Comparison of postmortem wholeâ€body contrastâ€enhanced microfocus computed tomography and highâ€field magnetic resonance imaging of human fetuses. Ultrasound in Obstetrics and Gynecology, 2022, 60, 109-117.	0.9	7
4	Comparative Analysis of Blood <scp>T₂</scp> Values Measured by <scp>T₂â€TRIR</scp> and <scp>TRUST</scp> . Journal of Magnetic Resonance Imaging, 2022, 56, 516-526.	1.9	6
5	Longitudinal CMR assessment of cardiac global longitudinal strain and hemodynamic forces in a mouse model of heart failure. International Journal of Cardiovascular Imaging, 2022, 38, 2385-2394.	0.2	1
6	Iron Oxide Nanoparticle Uptake in Mouse Brachiocephalic Artery Atherosclerotic Plaque Quantified by T2-Mapping MRI. Pharmaceutics, 2021, 13, 279.	2.0	7
7	Retrospective Cameraâ€Based Respiratory Gating in Clinical Wholeâ€Heart 4D Flow MRI. Journal of Magnetic Resonance Imaging, 2021, 54, 440-451.	1.9	5
8	Impairment of Cerebrovascular Hemodynamics in Patients With Severe and Milder Forms of Sickle Cell Disease. Frontiers in Physiology, 2021, 12, 645205.	1.3	16
9	The Antibiotic Doxycycline Impairs Cardiac Mitochondrial and Contractile Function. International Journal of Molecular Sciences, 2021, 22, 4100.	1.8	20
10	Quantification of Mouse Heart Left Ventricular Function, Myocardial Strain, and Hemodynamic Forces by Cardiovascular Magnetic Resonance Imaging. Journal of Visualized Experiments, 2021, , .	0.2	2
11	Double delay alternating with nutation for tailored excitation facilitates bandingâ€free isotropic highâ€resolution intracranial vessel wall imaging. NMR in Biomedicine, 2021, 34, e4567.	1.6	3
12	Coronary Flow Assessment Using Accelerated 4D Flow MRI With Respiratory Motion Correction. Frontiers in Bioengineering and Biotechnology, 2021, 9, 725833.	2.0	3
13	A Randomized Controlled Trial on the Effects of a 12-Week High- vs. Low-Intensity Exercise Intervention on Hippocampal Structure and Function in Healthy, Young Adults. Frontiers in Psychiatry, 2021, 12, 780095.	1.3	8
14	An iterative sparse deconvolution method for simultaneous multicolor ¹⁹ Fâ€MRI of multiple contrast agents. Magnetic Resonance in Medicine, 2020, 83, 228-239.	1.9	23
15	Compressed sensing MRI with variable density averaging (CS-VDA) outperforms full sampling at low SNR. Physics in Medicine and Biology, 2020, 65, 045004.	1.6	3
16	Hymenophore configuration of the oak mazegill (<i>Daedalea quercina</i>). Mycologia, 2020, 112, 895-907.	0.8	3
17	Altered brain fluid management in a rat model of arterial hypertension. Fluids and Barriers of the CNS, 2020, 17, 41.	2.4	12
18	High Spatiotemporal Resolution 4D Flow MRI of Intracranial Aneurysms at 7T in 10 Minutes. American Journal of Neuroradiology, 2020, 41, 1201-1208.	1.2	27

BRAM COOLEN

#	Article	IF	CITATIONS
19	Pseudoâ€spiral sampling and compressed sensing reconstruction provides flexibility of temporal resolution in accelerated aortic 4D flow MRI: A comparison with kâ€t principal component analysis. NMR in Biomedicine, 2020, 33, e4255.	1.6	17
20	Highly accelerated 4D flow cardiovascular magnetic resonance using a pseudo-spiral Cartesian acquisition and compressed sensing reconstruction for carotid flow and wall shear stress. Journal of Cardiovascular Magnetic Resonance, 2020, 22, 7.	1.6	33
21	Locally advanced rectal cancer: 3D diffusion-prepared stimulated-echo turbo spin-echo versus 2D diffusion-weighted echo-planar imaging. European Radiology Experimental, 2020, 4, 9.	1.7	2
22	Ultra-high resolution, 3-dimensional magnetic resonance imaging of the atherosclerotic vessel wall at clinical 7T. PLoS ONE, 2020, 15, e0241779.	1.1	3
23	Plaque Permeability Assessed With DCE-MRI Associates With USPIO Uptake inÂPatients With Peripheral Artery Disease. JACC: Cardiovascular Imaging, 2019, 12, 2081-2083.	2.3	24
24	Evaluation of compressed sensing MRI for accelerated bowel motility imaging. European Radiology Experimental, 2019, 3, 7.	1.7	11
25	Emerging Magnetic Resonance Imaging Techniques for Atherosclerosis Imaging. Arteriosclerosis, Thrombosis, and Vascular Biology, 2019, 39, 841-849.	1.1	32
26	Comparison of four MR carotid surface coils at 3T. PLoS ONE, 2019, 14, e0213107.	1.1	4
27	An isolated beating pig heart platform for a comprehensive evaluation of intracardiac blood flow with 4D flow MRI: a feasibility study. European Radiology Experimental, 2019, 3, 40.	1.7	8
28	Rapid T ₁ quantification from high resolution 3D data with modelâ€based reconstruction. Magnetic Resonance in Medicine, 2019, 81, 2072-2089.	1.9	30
29	Threeâ€dimensional diffusion imaging with spiral encoded navigators from stimulated echoes (3Dâ€DISPENSE). Magnetic Resonance in Medicine, 2019, 81, 1052-1065.	1.9	8
30	Insufficient slow-flow suppression mimicking aneurysm wall enhancement in magnetic resonance vessel wall imaging: a phantom study. Neurosurgical Focus, 2019, 47, E19.	1.0	36
31	Accelerated 4 <scp>D</scp> phase contrast <scp>MRI</scp> in skeletal muscle contraction. Magnetic Resonance in Medicine, 2018, 80, 1799-1811.	1.9	20
32	Vessel wall characterization using quantitative MRI: what's in a number?. Magnetic Resonance Materials in Physics, Biology, and Medicine, 2018, 31, 201-222.	1.1	35
33	Regional assessment of carotid artery pulse wave velocity using compressed sensing accelerated high temporal resolution 2D CINE phase contrast cardiovascular magnetic resonance. Journal of Cardiovascular Magnetic Resonance, 2018, 20, 86.	1.6	17
34	Diffusionâ€prepared stimulatedâ€echo turbo spin echo (DPstiâ€TSE): An eddy currentâ€insensitive sequence for threeâ€dimensional highâ€resolution and undistorted diffusionâ€weighted imaging. NMR in Biomedicine, 2017, 30, e3719.	1.6	25
35	Accelerated 4D selfâ€gated MRI of tibiofemoral kinematics. NMR in Biomedicine, 2017, 30, e3791.	1.6	13
36	Learningâ€based automated segmentation of the carotid artery vessel wall in dualâ€sequence MRI using subdivision surface fitting. Medical Physics, 2017, 44, 5244-5259.	1.6	15

BRAM COOLEN

#	Article	IF	CITATIONS
37	Evaluation of ultrasmall superparamagnetic iron-oxide (USPIO) enhanced MRI with ferumoxytol to quantify arterial wall inflammation. Atherosclerosis, 2017, 263, 211-218.	0.4	53
38	Investigations of Carotid Stenosis to Identify Vulnerable Atherosclerotic Plaque and Determine Individual Stroke Risk. Circulation Journal, 2017, 81, 1246-1253.	0.7	17
39	Diffusionâ€prepared neurography of the brachial plexus with a large fieldâ€ofâ€view at 3T. Journal of Magnetic Resonance Imaging, 2016, 43, 644-654.	1.9	14
40	Threeâ€dimensional quantitative T ₁ and T ₂ mapping of the carotid artery: Sequence design and in vivo feasibility. Magnetic Resonance in Medicine, 2016, 75, 1008-1017.	1.9	43
41	Magnetic Resonance Imaging–Derived Renal Oxygenation and Perfusion During Continuous, Steadyâ€State Angiotensinâ€II Infusion inÂHealthy Humans. Journal of the American Heart Association, 2016, 5, e003185.	1.6	23
42	HDL mimetic CER-001 targets atherosclerotic plaques in patients. Atherosclerosis, 2016, 251, 381-388.	0.4	51
43	PCA-based groupwise image registration for quantitative MRI. Medical Image Analysis, 2016, 29, 65-78.	7.0	118
44	Noninvasive Differentiation between Hepatic Steatosis and Steatohepatitis with MR Imaging Enhanced with USPIOs in Patients with Nonalcoholic Fatty Liver Disease: A Proof-of-Concept Study. Radiology, 2016, 278, 782-791.	3.6	50
45	Three-dimensional dynamic contrast-enhanced MRI for the accurate, extensive quantification of microvascular permeability in atherosclerotic plaques. NMR in Biomedicine, 2015, 28, 1304-1314.	1.6	30
46	Quantitative T ₂ mapping of the mouse heart by segmented MLEV phase ycled T ₂ preparation. Magnetic Resonance in Medicine, 2014, 72, 409-417.	1.9	30
47	Myocardial perfusion MRI shows impaired perfusion of the mouse hypertrophic left ventricle. International Journal of Cardiovascular Imaging, 2014, 30, 619-628.	0.7	12
48	Non-rigid Groupwise Image Registration for Motion Compensation in Quantitative MRI. Lecture Notes in Computer Science, 2014, , 184-193.	1.0	4
49	High frame rate retrospectively triggered Cine MRI for assessment of murine diastolic function. Magnetic Resonance in Medicine, 2013, 69, 648-656.	1.9	23
50	Passive targeting of lipidâ€based nanoparticles to mouse cardiac ischemia–reperfusion injury. Contrast Media and Molecular Imaging, 2013, 8, 117-126.	0.4	28
51	Quantitative firstâ€pass perfusion MRI of the mouse myocardium. Magnetic Resonance in Medicine, 2013, 69, 1735-1744.	1.9	23
52	Accelerated highâ€frameâ€rate mouse heart cineâ€MRI using compressed sensing reconstruction. NMR in Biomedicine, 2013, 26, 451-457.	1.6	17
53	Embryonic Cardiomyocyte, but Not Autologous Stem Cell Transplantation, Restricts Infarct Expansion, Enhances Ventricular Function, and Improves Long-Term Survival. PLoS ONE, 2013, 8, e61510.	1.1	17
54	Distribution of lipid-based nanoparticles to infarcted myocardium with potential application for MRI-monitored drug delivery. Journal of Controlled Release, 2012, 162, 276-285.	4.8	69

BRAM COOLEN

#	Article	IF	CITATIONS
55	Efficacy of positive contrast imaging techniques for molecular MRI of tumor angiogenesis. Contrast Media and Molecular Imaging, 2012, 7, 130-139.	0.4	6
56	Contrastâ€enhanced MRI of murine myocardial infarction – Part II. NMR in Biomedicine, 2012, 25, 969-984.	1.6	18
57	Contrastâ€enhanced MRI of murine myocardial infarction – Part I. NMR in Biomedicine, 2012, 25, 953-968.	1.6	16
58	Regional contrast agent quantification in a mouse model of myocardial infarction using 3D cardiac T1mapping. Journal of Cardiovascular Magnetic Resonance, 2011, 13, 56.	1.6	17
59	Threeâ€dimensional <i>T</i> ₁ mapping of the mouse heart using variable flip angle steadyâ€state MR imaging. NMR in Biomedicine, 2011, 24, 154-162.	1.6	58
60	Mouse myocardial firstâ€pass perfusion MR imaging. Magnetic Resonance in Medicine, 2010, 64, 1658-1663.	1.9	43
61	On the use of steady-state signal equations for 2D TrueFISP imaging. Magnetic Resonance Imaging, 2009, 27. 815-822.	1.0	6